Hyperfine Interact (2016) 237: 117
DOI 10.1007/s10751-016-1326-1

CrossMark

Growth of Ga_2O_3 by furnace oxidation of GaN studied by perturbed angular correlations

Michael Steffens[1,2] · **Reiner Vianden**[2] · **Alberto F. Pasquevich**[3,4]

Published online: 10 August 2016
© Springer International Publishing Switzerland 2016

Abstract Ga_2O_3 is a promising material for use in "solar-blind" UV-detectors which can be produced efficiently by oxidation of GaN. In this study we focus on the evolution of the oxide layer when GaN is heated in air. The experimental method applied is the perturbed angular correlation (PAC) spectroscopy of γ-rays emitted by radioactive nuclides, here ^{111}Cd and ^{181}Ta, whose parent nuclei are ion implanted into films of GaN grown on sapphire. As the emission pattern for nuclei in GaN is clearly distinct from that of nuclei in Ga_2O_3, the fraction of probe nuclei in the oxide layer can be directly measured and allows to follow the time dependent growth of the oxide on a scale of less than 100 nm. Additional measurements were carried out with the oxidized sample held at fixed temperatures in the temperature range from 19 K to 973 K showing transitions between the hyperfine interactions of ^{111}Cd in the oxide matrix both at high and low temperatures. A model for these transitions is proposed.

Keywords Perturbed angular correlation spectroscopy · TDPAC · Gallium nitride · Gallium oxide · Self-trapped hole · Furnace oxidation

---

This article is part of the Topical Collection on *Proceedings of the International Conference on Hyperfine Interactions and their Applications (HYPERFINE 2016), Leuven, Belgium, 3-8 July 2016*

✉ Michael Steffens
michael.steffens@int.fraunhofer.de

[1] Fraunhofer Institute for Technological Trend Analysis INT, Appelsgarten 2, 53879 Euskirchen, Germany

[2] Helmholtz - Institut für Strahlen- und Kernphysik der Universität Bonn, Nussallee 14-16, 53115 Bonn, Germany

[3] Departamento de Física, IFLP, Facultad de Ciencias Exactas, Universidad Nacional de La Plata, 1900 La Plata, Argentina

[4] Comisión de Investigaciones Científicas de la Provincia de Buenos Aires, La Plata, Argentina

1 Introduction

Ga_2O_3 is a transparent wide band gap semiconductor which can be used for high-efficiency, "solar blind" UV photodetectors. However, the controlled production of high quality films of monoclinic β-Ga_2O_3 which are essential for the fabrication of such detectors is still difficult. In a recent study Weng et. al. [1] presents a feasible and efficient way to grow Ga_2O_3 by furnace oxidation of GaN. This is an important step forward since thermal oxidation is a simple, cheap and clean process. In this study we focus on the details of the evolution of the oxide layer when oxidized at 1223 K in dry air. The experimental method applied is the perturbed angular correlation (PAC) technique of γ-rays emitted by probe nuclides, here ^{111}In and ^{181}Hf, which are ion implanted into the GaN samples [2]. It allows to measure the electric field gradient (EFG) at the crystal site of the probe nuclei. Since the EFG for nuclei in GaN is clearly distinct from that of nuclei in Ga_2O_3, the fraction of probe nuclei in the oxide layer can be directly measured. This allows us to follow the time dependent growth of the oxide on a scale of less than 100 nm and at the same time monitor the quality of the crystal lattice in the vicinity of the probe nuclei. Since they are not uniformly distributed inside the sample, the layer thickness has to be deduced by comparing the measurement results with the lateral distribution of nuclei.

2 Experimental technique and data analysis

The PAC probes ^{111}In ($T_{1/2} = 2.8$ d) and ^{181}Hf ($T_{1/2} = 42.4$ d) decay by electron capture (EC) to ^{111}Cd and β^--decay to ^{181}Ta, respectively. In both cases an excited state of the daughter nuclide is populated and decays further by emission of a γ-γ-cascade, passing a spin-5/2 state. The half life of this intermediate state is $T_{1/2} = 85$ ns for ^{111}Cd and $T_{1/2} = 10.8$ ns for ^{181}Ta [3, 4]. The hyperfine interaction of the EFG produced by the charge distribution in the crystal lattice with the quadrupole moment of the nuclear state is detected by the PAC technique.

The emission directions of the two γ in the γ-γ-cascade are correlated by $W(\Theta)$. When subjected to an EFG, transitions between the hyperfine levels of the spin-5/2 intermediate state introduce a time modulation of the angular correlation pattern by a perturbation factor $G_{kk}(t)$:

$$W(\Theta, t) = \sum_{k=0}^{3} A_{kk} G_{kk}(t) P_k(\cos \Theta) \tag{1}$$

with the anisotropy coefficient A_{kk} depending upon the multipolarities and spins of the decay transitions. $P_k(\cos \Theta)$ are Legendre polymomials.

$$G_{kk} = s_{k0} + \sum_{n=1}^{3} s_{kn} \cos(\omega_n(\eta)\, t) \cdot e^{-\delta \omega_n(\eta) t} \tag{2}$$

The ω_n are the transition frequencies between the hyperfine sublevels of the intermediate state which depend on the asymmetry parameter η and the spin-independent quadrupole interaction constant ν_q of the EFG:

$$\nu_q = \frac{eQV_{zz}}{h} \qquad \eta = \frac{V_{xx} - V_{yy}}{V_{zz}}, \tag{3}$$

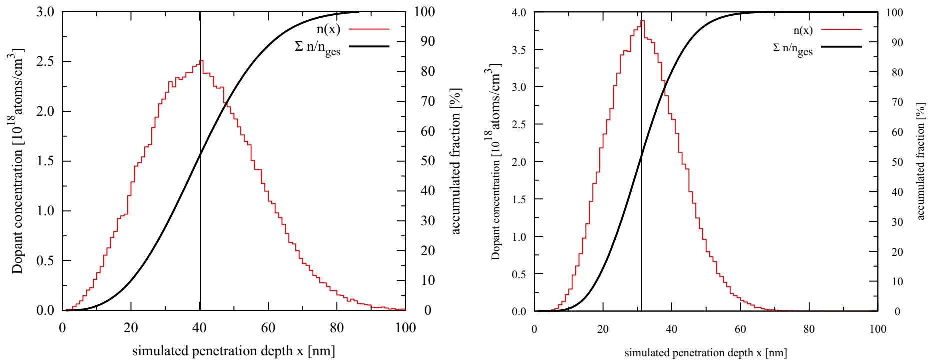

(a) SRIM simulation of Indium in GaN (b) SRIM simulation of Hafnium in GaN

Fig. 1 Estimated depth profiles of ^{111}In and ^{181}Hf implanted in GaN with ion energy of 160 keV. The *red lines* show the lateral distribution of the dopant concentration versus depth (*left* hand scale). These curves are simulated using SRIM 2012. The *black lines* give the fraction of all ions situated at depth x or less (*right* hand scale)

where V_{xx}, V_{yy} and V_{zz} are the components of the diagonalized EFG tensor. A Lorentzian frequency distribution with relative width δ is taken into account by the exponential in (2). For the remainder of this article, the quadrupole interaction constant ν_q will be used.

In our experiments we measure the angular correlation using a conventional four-detector fast-slow coincidence set-up with LSO scintillation detectors [5, 6]. For each measurement 12 coincidence spectra were collected with relative angles of $\theta = 90°$ or $180°$ between the emission directions of the γ rays. The coincidence spectra contain information on the number of nuclear decays measured with a delay time t between both γ rays observed in a given detector combination. Thus, each detected decay contributes one count to the corresponding coincidence spectrum. Each spectrum contains statistical information of typically 10^6 probe nuclei.

We get the perturbation factor by calculating the ratio

$$R(t) = 2\frac{\overline{W}(180°, t) - \overline{W}(90°, t)}{\overline{W}(180°, t) + 2\overline{W}(90°, t)} \approx \sum_i f_i A_{22}^i G_{22}^i \quad (4)$$

where $\overline{W}(\theta, t)$ is the geometric mean of all spectra with relative angle θ. In (4) it is already taken into account that i distinct hyperfine interactions due to different electronic environments may exist in the sample, with a fraction f_i of the probe nuclei subjected to these.

3 Sample preparation and oxidation

6 μm thick GaN grown on saphire was ion implanted with either ^{111}In or ^{181}Hf at the Bonn isotope separator (BONIS) with an implantation energy of 160 keV each.

For these conditions, Monte Carlo simulations with SRIM [7] show the maximum of the ion distribution profile at a depth of 40 nm for ^{111}In and 25 nm for ^{181}Hf (Fig. 1). Nearly all probe ions are deposited within 100 nm and 70 nm beneath the surface, respectively. Their

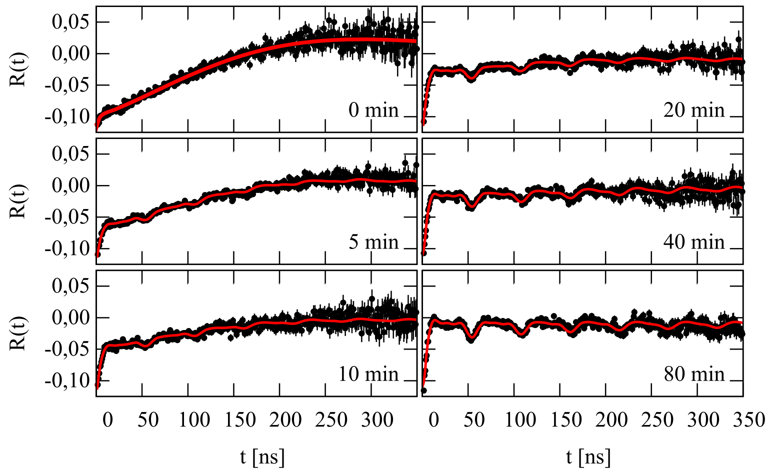

Fig. 2 Selected spectra of ^{111}Cd following the oxidation of GaN to Ga_2O_3

decay products ^{111}Cd and ^{181}Ta, are the PAC probes at which the hyperfine interaction is measured, so the PAC measurements should be extremely sensitive to the early development of the oxide.

Rapid thermal annealing at 1273(3) K for 2 min in nitrogen atmosphere removes most of the damage due to the ion implantation as can be shown with PAC measurements after the annealing. These are indicated by 0 min oxidation time in Figs. 2 and 3. A second piece of GaN used as proximity cap helps to suppress nitrogen diffusion out of the sample. At these temperatures, diffusion of the implanted nuclei should be negligible [8].

Immediately before the first oxidation step, the surface of the sample is wet etched with diluted hydrochloric acid for 3 min to remove the native oxide [9]. There was no contamination of the diluted acid with ^{111}In, so it can be assumed that the GaN layer is not affected by this procedure as was recently shown by Zhuang et al. [10].

For the oxidation, the sample is placed in a tube furnace preheated to 1223(3) K to prevent a reformation of the native oxide layer during temperature increase. The oxygen for the chemical reaction

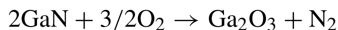

$$2GaN + 3/2O_2 \rightarrow Ga_2O_3 + N_2$$

is simply provided by the ambient air.

Oxidation steps of 5 min each were performed followed by PAC measurements at room temperature to study the development of the oxide. The overall oxidation time was chosen such that the volume containing the PAC probes was completely oxidized as indicated by the results of the measurements. For ^{111}In, an oxidation time of 80 min was more than sufficient, so the measurements with ^{181}Hf were stopped after 70 min already. This procedure proved reproducible with various samples and independent of the length of the individual oxidation steps.

Additional measurements were carried out in vacuum with the oxidized sample held at fixed temperatures in the temperature range from 19 K to 973 K. A furnace similar to the one presented in [11] was used for measurements at or above room temperature and a commercial cryostat for measurements at low temperatures.

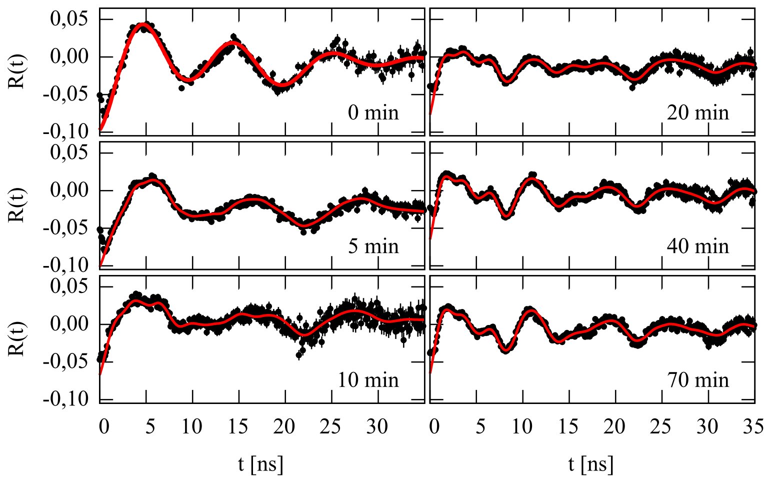

Fig. 3 Selected spin precession curves of ^{181}Ta following the oxidation of GaN to Ga_2O_3

4 Results

After the annealing step described above, 84(3) % of the Cd probes show the quadrupole interaction constant characteristic for probes on regular, undisturbed Ga sites in GaN. This value is in good agreement with previous studies [12]. For Ta, however, it is only about half of what would be reached normally, noticeable in the anisotropy at $t = 0$ ns in Fig. 3. This is due to an unusually high dose of stable Hf which had contaminated the ^{181}Hf ion beam during the implantation. Thus, about half of the Hf are situated either in lattice sites strongly disturbed by neighboring Hf atoms or in regions amorphized by the implantation, leading to a large quadrupole interaction constant, which cannot be resolved by the PAC set-up. This fraction does not anneal and shows no involvement in the oxidation. Therefore, in the following analysis only the fraction of Ta probes on regular Ga sites is considered.

Selected spectra following the development of the oxide with oxidation time are presented in Figs. 2 and 3 for ^{111}In and ^{181}Hf, respectively. Least square fits of (2) to the data yield the fraction of probes in different surroundings given by distinct hyperfine interactions in the sample. The prominent fractions resulting from the fits are shown in Fig. 4.

4.1 Identification of the contributing interactions

First we will identify the hyperfine interactions (HFIs) in GaN and Ga_2O_3. The characteristics of these HFIs are compiled in Table 1, together with their development with oxidation time.

Before the start of the oxidation process, the predominant HFI can be attributed to ^{111}Cd or ^{181}Ta on Ga locations in the regular GaN matrix (Cd_{Ga}(N) and Ta_{Ga}(N), respectively) [13–15]. The EFGs associated with these interactions are both axially symmetric ($\eta = 0$) and single crystalline.

In the Ta-implanted sample, one prominent interaction emerges with oxidation time which we identify with ^{181}Ta on the Ga_{II} lattice site in Ga_2O_3 [16] (Ta_{Ga}(Ox)). As it is known in the literature [17–19], atoms with a significantly larger ionic radius than Ga, such

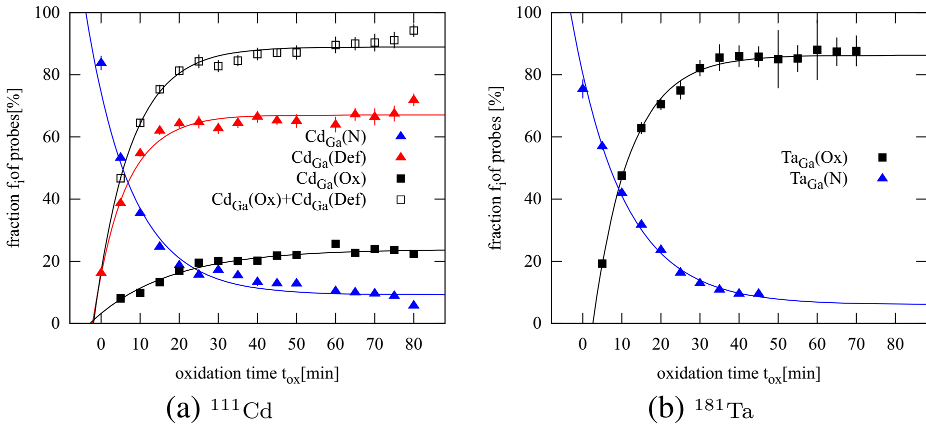

Fig. 4 Development of the probe fractions with oxidation time. The fraction of probes in the nitride show an exponential decay with both types of probes. While there is only one interaction (Ta_{Ga}(Ox)) associated with the oxide for ^{181}Ta, there are two for ^{111}Cd: one given by probes in the nominal defect free lattice (Cd_{Ga}(Ox)) and one highly attenuated interaction (Cd_{Ga}(Def)) which we assume to be related to probes in Ga_2O_3 accompanied by electronic defects. Assuming both of these interactions to represent probes in the oxide matches roughly the oxide growth for the ^{181}Ta implanted sample. Lines are given to guide the eye

as In or Hf, can substitute Ga only on this Ga_{II} sites in Ga_2O_3. After 70 min of oxidation 88(5) % of the probes are in this environment.

Two point defect related interactions are present in the Hf-implanted samples with one being only present after annealing and is most likely due to implantation damage not properly annealed. The second point defect (Ta_{Ga}(Def)), present at all stages of the oxidation and only noticeable in the first nanoseconds of the spin precession curves, shows the characteristics of intrinsic defects of GaN [15, 20].

With ^{111}Cd however, two distinct interactions can be associated with the probes on Ga_{II} sites. One clearly defined interaction (Cd_{Ga}(Ox)), present at 27(5) % of probes after oxidation, is the interaction of ^{111}In in a nominal and defect-free Ga_2O_3 matrix [18, 19].

The second, strongly attenuated interaction is present at 64(6) % of probes after oxidation (Cd_{Ga}(Def)). The stronger attenuation can be seen in the spectra at larger delay times t. We will assume that this interaction is present at nuclei on Ga_{II} sites with nearby electronic defects [18, 19] and we identify both Cd_{Ga}(Ox) and Cd_{Ga}(Def) with ^{111}Cd in the oxide. The fraction of probes in a Ga_2O_3 matrix is then given by the sum of the fractions of the two HFIs. We will validate this assumption later in this article by showing, that by variation of the sample temperature, Cd_{Ga}(Def) can be reversibly switched to Cd_{Ga}(Ox) and vice versa.

4.2 Evolution of the oxide layer with oxidation time

Due to the conversion of the nitride, the fraction f_N of probes in this environment (X_{Ga}(N), with X being either Cd or Ta) decreases with oxidation time (Fig. 4), which can phenomenologically described by a falling exponential $f_N(t) = A + f_N(t = 0) \cdot e^{-t/\tau_N}$, with $\tau_N = 12(2)$ min for ^{111}Cd and 13(1) min for ^{181}Ta.

The development of the oxide gives rise to Ta_{Ga}(Ox) and both Cd_{Ga}(Ox) and Cd_{Ga}(Def) with oxidation time. The sum of the corresponding probe fractions (f_{ox}(Cd) and f_{def}(Cd)) is shown in Fig. 4 as open squares. For both probes this can be described as $f_{Ox}(t) =$

Table 1 Time frames of the oxidation for measurements with ^{111}Cd and ^{181}Ta

	time frame [min]	f_i [%]	ν_Q [MHz]	η	δ [%]
Cd$_{\text{Ga}}$(N)	0 - 20	84 $\rightarrow$ 19	5.4(2)	0	55(1)
	> 20	16 $\rightarrow$ 6	5.4 $\rightarrow$ 0.5	0	60 $\rightarrow$ 355
Cd$_{\text{Ga}}$(Ox)	0 - 20	0 $\rightarrow$ 17	123.9(5)	0.13(3)	3.0(4)
	> 20	17 $\rightarrow$ 23			
Cd$_{\text{Ga}}$(Def)	0 - 20	16 $\rightarrow$ 65	127(10)	0.8 $\rightarrow$ 0.35	130 $\rightarrow$ 100
	> 20	66(3)	162(10)	0.35(2)	83(10)
Ta$_{\text{Ga}}$(N)	0 - 30	75 $\rightarrow$ 10	290 $\rightarrow$ 345 [$t \geq 5$ min]	0	10(2)
	35 - 45			0.19 $\rightarrow$ 0.59	
	> 45	–	–	–	–
Ta$_{\text{Ga}}$(Ox)	0 - 30	0 $\rightarrow$ 82	743(9)	0.41(3)	7(2)
	35 - 45	86(2)			
	> 45				
Ta$_{\text{Ga}}$(Def)	5 - 30	6(3)	1230(53)	0.95(6)	4(3)
	35 - 45				
	> 45	13(2)			18(4)
HFI$_{\text{impl}}$	0-10	25 $\rightarrow$ 7	256(12)	0.75(9)	31 $\rightarrow$ 1

These are mainly given by the changes to the interaction in the nitride environment. The values presented show either clear tendencies of the parameters (indicated by $\rightarrow$) or, if nearly constant, give the average and standard distribution of the parameters. Characteristics which are deemed identical over different time ranges are highlighted in gray color

$B + f_{\text{Ox}}(t = 0) \cdot \left(1 - e^{-t/\tau_{\text{Ox}}}\right)$ giving $\tau_{\text{Ox}}(\text{Cd}) = 9.3(8)$ min and $\tau_{\text{Ox}}(\text{Ta}) = 9.5(3)$ min. Associating both Cd$_{\text{Ga}}$(Ox) and Cd$_{\text{Ga}}$(Def) with ^{111}Cd in the Ga_2O_3 matrix, we get a time dependence of the Ga_2O_3 layer evolution similar to ^{181}Ta.

4.3 Reversible switching of interactions with temperature in ^{111}Cd implanted samples

The temperature dependent measurements were carried out with two new samples prepared as described above, due to the comparatively short half-life of ^{111}In. One sample was used solely for high temperature measurements up to 973 K in a PAC furnace [11]. With another sample, measurements were made covering the full temperature range from 19 K to 973 K. For comparison, measurements with ^{181}Ta at high temperatures were performed with the same sample used for oxidation measurements in the previous section.

Figure 5 shows some selected spin precession curves for the Cd-implanted samples. As we focus on probes in the oxide layer, Fig. 6a and b show only the fraction of probes in either X$_{\text{Ga}}$(Ox) or X$_{\text{Ga}}$(Def) so the sum of the fractions shown does not necessarily add up to 100 %.

The thermal history of the samples starts at RT with increasing temperature until reaching 973 K, decreasing T to RT and for sample 3 continuing at 19 K until arriving again at RT.

Although to a different extent, both sample 2 and 3 show an increase of Cd$_{\text{Ga}}$(Ox) with sample temperature starting at approx. 600 K, which reversibly reduces when returning to RT. A similar, although less pronounced, increase is seen at temperatures below 200 K. At both high and low temperatures a lesser fraction of probes are subjected to Cd$_{\text{Ga}}$(Def). If this was due to some change in crystalline structure, we would expect a similar behavior for ^{181}Ta. And although there seems to be a slight increase of Ta$_{\text{Ga}}$(Ox) when stepping up in temperature (Fig. 6c), the uncertainties coming from the least square fits prevent any

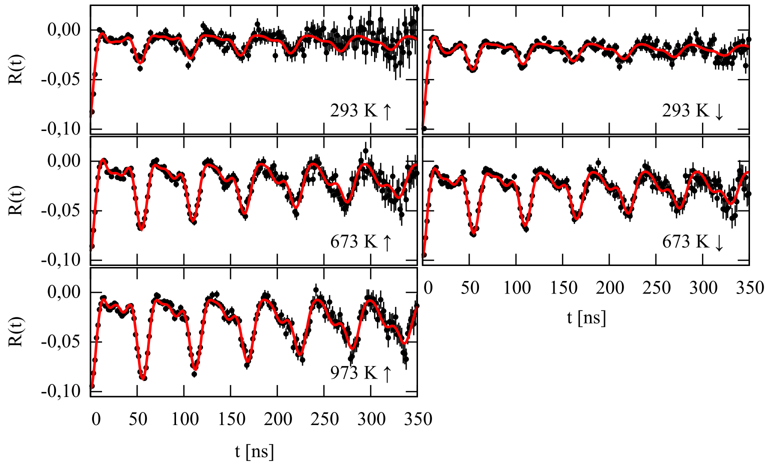

(a) Furnace measurements between room temperature (RT) and 973 K

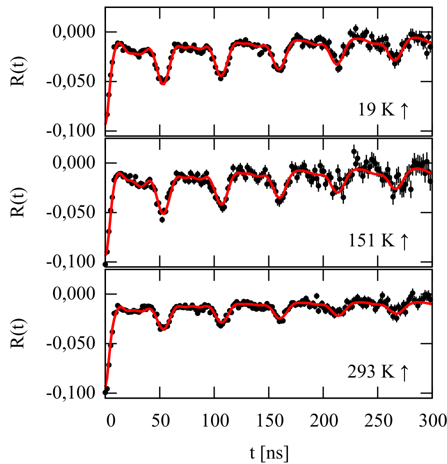

(b) Cryostat measurements between 18 K and RT

Fig. 5 Spin precession curves for the temperature dependent measurements of ^{111}Cd in a Ga_2O_3 layer formed by GaN-oxidation. Between the measurements the sample temperature was first raised in steps of 100 K (indicated by ↑) and after the measurement at 973 K lowered in similar steps (indicated by ↓)

concise conclusion. Within errors we see therefore no significant thermal behavior for the ^{181}Ta probes.

We conclude that Cd_{Ga}(Def) is an electronic defect coupled to ^{111}Cd which can detrap thermally to be responsible for the switching between Cd_{Ga}(Ox) and Cd_{Ga}(Def) with temperature. As previously assumed, both interactions should thus belong to nuclei in the oxide matrix, one with and one without this coupled electronic defect.

While thermal detrapping may explain the high temperature branch and is consistent with previous models [18, 19], this does not explain the rise of Cd_{Ga}(Ox) at low temperatures. We will present a detailed model for both the high and low temperature behavior in the discussion.

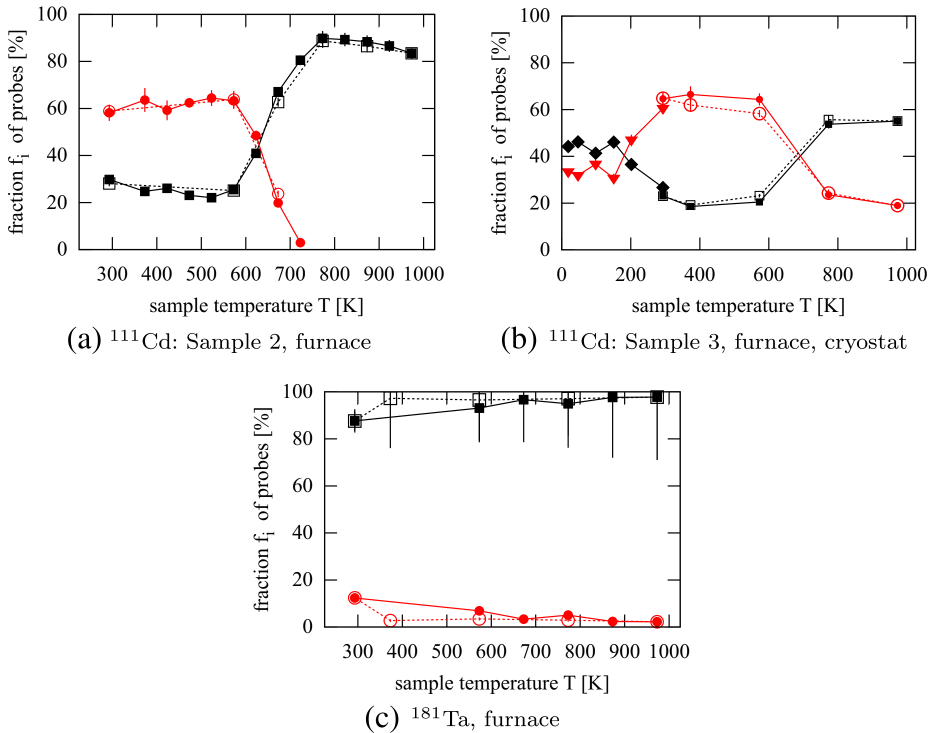

Fig. 6 Probe fractions in X_{Ga}(Ox) and X_{Ga}(Def) during temperature dependent measurements with two ^{111}Cd implanted samples and one ^{181}Ta-implanted sample. Both Cd-implanted samples show the same characteristics after oxidation at RT and both samples show a recovery of X_{Ga}(Ox) at high temperatures. With one sample **a** however this recovery is significantly more pronounced. The Ta-implanted sample shows no major changes within errors to the HFI at elevated temperatures. *Lines* are given to guide the eye. The symbols indicate the thermal history with filled symbols for increasing and *open symbols* for decreasing temperatures

5 Discussion

5.1 Evolution of the oxide layer with oxidation time

As shown above, perturbed angular correlations can give the fraction of implanted probe atoms in distinct lattice or electronic environments. We can thus derive the fraction of probes still in a GaN environment and of probes in the Ga_2O_3 layer of the sample for each step of the oxidation process. In case of probe ^{181}Ta this information is simply given by the fraction of probes in Ta_{Ga}(Ox). For ^{111}Cd we assume the combination of Cd_{Ga}(Ox) and Cd_{Ga}(Def) to be a valid representation. GaN will oxidize to Ga_2O_3 externally, i.e. the oxide layer will start forming on top of the sample and continue to grow following an oxidation front into the sample. Hence it should be possible to estimate the position of the oxidation front with time. For this, we take the experimental probe fractions at a certain oxidation time (Fig. 6) and relate these to the accumulated fraction of probes up to a certain depth in the source material (Fig. 1). When no oxide has formed yet, the position of the oxidation front is set to 0 nm with higher values indicating the penetration depth of the oxidation front in the source material. This is not equivalent to an estimation of the oxide thickness, as this would require

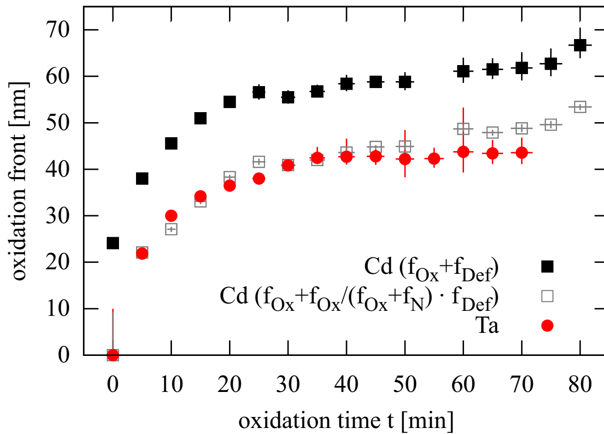

Fig. 7 Estimate of the oxidation front progression with oxidation time. The approach and its limitations are discussed in the text. The time dependence of the oxidation should be independent of the implanted probes. For ^{111}Cd we only get results comparable to ^{181}Ta if we scale the defectuous environment, as this is already present in the nitride

detailed knowledge about the microscopic restructuring of the material, the resulting lattice structure and parameters, all of which is not accessible by PAC alone.

As was mentioned earlier, the probes are not deposited homogeneously in the samples and due to this, estimating the position of the oxidation front has to rely on the simulation data of the probe distributions given by SRIM. For GaN the depth profile of implanted species should be well estimated by SRIM and very little prone to diffusion during annealing [8]. But, due to the inhomogeneous distribution, once a large majority of probes are inside the oxidized region, small uncertainties in the experimental probe fraction translate to large uncertainties in the estimated position.

The result of this estimation is given by the filled symbols in Fig. 7 and indicates a more than 20 nm layer already present in the Cd-implanted sample before oxidation, as the interaction Cd_{Ga}(Def) is already present at this stage. At larger oxidation times there would be a corresponding offset for that sample as compared to the Ta-implanted sample.

If we assume, that Cd_{Ga}(Def) represents both a highly damped defect in the nitride as well as in the oxide that cannot be separated in our least square fits as their characteristics are very similar, we get the open symbols in Fig. 7. For this, we scale the fraction f_{def} according to the magnitude of the probe fraction in oxide environment, i.e. we calculate $f_{def} \cdot f_{ox}/(f_{ox}+f_N)$ and add that to f_{ox}. By definition the oxide vanishes at oxidation time 0 min, but we also get a fine match between the oxidation process in this estimation and the process in the Ta-implanted sample.

5.2 Model for the reversible switching of interactions with temperature in ^{111}Cd implanted samples

After oxidation, we assume both interactions Cd_{Ga}(Ox) and Cd_{Ga}(Def) to represent Cd probes on Ga_{II} lattice sites in the oxide. The first is in good agreement with the literature [18, 19] and the latter can be at least reduced, in one sample even switched off, just by raising the temperature to the samples. To show this reversible switching more clearly, we calculated $f^*_{ox} = f_{ox}/(f_{ox} + f_{def})$ which is the ratio of Cd on defect-free Ga_{II} lattice sites

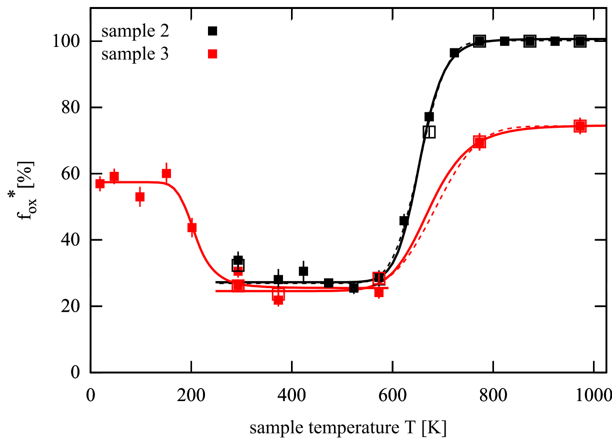

Fig. 8 The fraction of ^{111}Cd under the non-attenuated Cd_{Ga}(Ox) is set into relation to all Cd-probes in the oxide layer (Cd_{Ga}(Ox)+Cd_{Ga}(Def)). The so calculated reduced fraction f_{ox}^* shows a minimum from approximately RT to 600 K for both samples under investigation. At least for high temperatures this is reversible independent of the thermal history (*closed symbols* and *solid lines* indicate increasing and *open symbols* and *dashed lines* indicate decreasing temperatures). Although the extent is different for the two samples under investigation, variation of the sample temperature allows to alter the predominant HFI for the majority of probes in both samples. *Lines* are given to guide the eye

to all Cd on Ga_{II} lattice sites in the oxide (Fig. 8). The so calculated reduced fraction f_{ox}^* shows a minimum from approximately RT to 600 K for both samples under investigation. Although the extent is different for the two samples under investigation, variation of the sample temperature allows to reversibly alter the predominant HFI for the majority of probes in both samples. The thermal activation energies for these transitions are 19(1) meV for the low temperature transition and 56(1) meV or 59(3) meV, respectively, for the two samples at high temperatures.

An electron hole coupled to the Cd-probes is the most likely electronic defect. The ^{111}In on Ga sites are embedded isovalent in the 3^+ charge state in the oxide [17, 21]. During the EC-decay to ^{111}Cd, an initial hole is created in an inner shell of the probe, which relaxes to the valence band. An additional undefined number of holes are generated by accompanying Auger processes, leaving the nuclei in a much higher charge state [22, 23]. These holes can recombine with free electrons, are thus mobile and in a semiconducting material the relaxation process is expected to be resolved on a pico-second time frame [24]. Unless an at least meta-stable defect with lifetimes of tens of nanoseconds is formed, these holes cannot perturb the ^{111}Cd intermediate state.

Although proposed for some time [27], it was only recently established that Ga_2O_3 can form self-trapped holes (STH) [25, 28, 29]. These are local lattice distortions generated by a hole which are energetically more favorable on a local scale than the non-distorted lattice and can thus trap the hole generating the distortion, introducing a stable defect state in the band gap. The most prominent experimental effect attributed to these STH is an UV emission band in the photo luminescence spectrum [25, 28, 29]. A certain activation energy E_B is required for the free hole to be trapped. Such defects can become mobile again when passing another, significantly higher potential barrier (E_B + E_{ST}). Figure 9 is an adaptation of the formation model from Varley et al. [25], who could show the formation of these defects in Ga_2O_3 with ab-initio calculations. In these calculations a free valence band

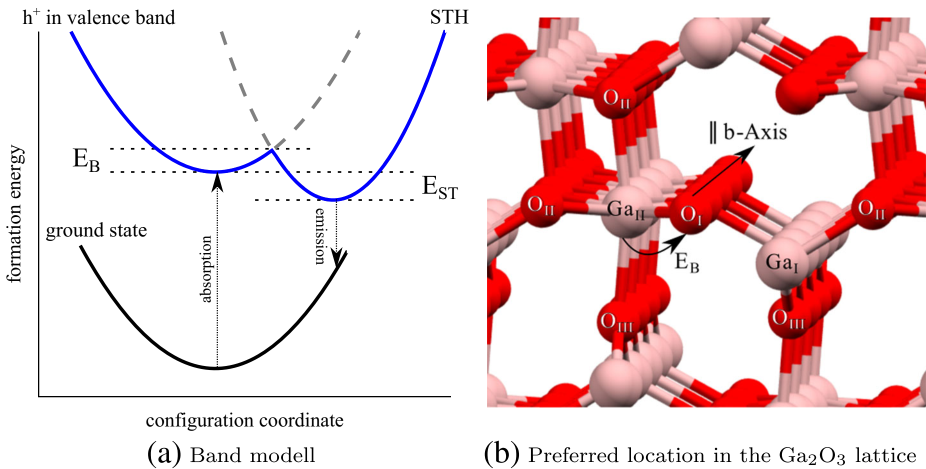

Fig. 9 **a** depicts a model for the formation energy of a self-trapped hole (STH) in relation to an abstract coordination number, which describes local lattice deformations. The STH lies energetically lower by E_{ST} compared to a free valence band hole. The STH forms when the potential barrier of E_B is passed. In Ga_2O_3 this is equivalent to a tunneling of the hole from Ga_{II} to the next neighbor O_I (here figure **b** shows the unperturbed Ga_2O_3 lattice). The potential barrier for jumps parallel to the crystal b-axis along equivalent lattice positions is less than $E_{ST}+E_B$, making this the preferred diffusion path. (based on the model and simulations in [25], lattice coordinates from [26])

hole stabilizes only at O_I next to Ga_{II} sites after passing a potential barrier of 0.1 eV. The corresponding distortion of the lattice around this site was calculated to be around 8 % (see supplemental material of [25]). The STH can escape with an activation energy of 0.63 eV to move back to the Ga site or with 0.4 eV when moving to equivalent oxygen positions along the crystal b-axis.

If these activation energies could be provided purely thermally, this could explain the higher fraction of defect-free probes at low temperatures and the transition with increasing temperature starting above 150 K. The second transition at higher temperatures starting around 600 K could then be attributed to the mobilization of the STH, which is in line with the previous models of holes localized next to the probes provided in the literature [18].

The thermal activation energies deduced from the experiments, 19(1) meV for the low temperature and 56–59 meV for the high temperature transition, are significantly lower than the energies required for formation or relaxation in [25]. But in our case we are not in a pristine Ga_2O_3 lattice, but in a lattice doped with In/Cd probes. From ab-initio calculations by Blanco et al. [17], local lattice distortions of 0.15 Å (approx. 7 % of next neighbor bond lengths) are already expected around Indium on Ga_{II} sites and we would expect even larger distortions after the EC-decay due to the higher cadmium charge state in the lattice. Further, a free valence band hole would not have to be trapped next to the probe, as the probes would generate adjacent holes during the EC-decay. Both mechanisms could facilitate the formation or relaxation of the STH and thus lower the corresponding activation energies.

This model would not apply to ^{181}Ta in Ga_2O_3, as the tantalum charge state 5^+ being positive relative to the lattice would suppress the coupling of holes to the probe.

We propose this model of post-EC hole trapping in the distorted lattice around In/Cd probes, with activation energies for formation and relaxation of this stable defect realized purely thermally, to explain the increased fraction of probes in a defect-free Ga_2O_3 matrix

both at temperatures higher and lower than room temperature. While at higher temperatures an increase of free electrons can contribute to the relaxation, for low temperatures we can rule out jump-diffusion mechanisms, as we would expect these to be suppressed by phonon-interaction at temperatures significantly below 150 K. So we know of no other model to describe the low temperature behavior satisfyingly.

Varley et al. [25] carried out further ab-initio calculations showing STH formation in Al_2O_3, TiO_2, SnO_2, In_2O_3 and MgO, most of which show similar high temperature defect relaxation with PAC using ^{111}Cd [30], and no STH formation in ZnO and SiO_2, which do not show this effect in PAC measurements with ^{111}Cd. Here Ga_2O_3 and In_2O_3 show the highest tendency for STH formation. Low-temperature PAC measurements of all of these materials are sparsely published, so it would be interesting to check whether some of the materials also show the increase of defect-free interactions at low temperatures and whether this model could also be applicable to these materials.

6 Summary and conclusions

In this article, we follow the evolution of the Ga_2O_3 oxide layer by furnace oxidation of GaN with the experimental method of perturbed angular correlations. Experiments are performed at room temperature in between oxidation steps. The probe nuclei ^{111}Cd and ^{181}Ta are introduced into 6 μm thin nitride layers grown on sapphire by ion implantation of the parent nuclei ^{111}In and ^{181}Hf. Both types of probes are incorporated on substitutional Ga sites in the lattice.

Over the course of the oxidation we see a decrease of the signal from probes in the nitride and an increase of the corresponding signal in the oxide. While for ^{181}Ta this is represented by a single hyperfine interaction (Ta_{Ga}(Ox)), we attribute two disctinct interactions for ^{111}Cd on Ga_{II} sites in the oxide (Cd_{Ga}(Ox) and Cd_{Ga}(Def)).

Regarding the temporal evolution of the oxide, we estimate the position of the oxidation front in the material with time by correlating the fractions of probe nuclei in the oxide matrix with the SRIM-simulated implantation profiles. While this gives reasonable results with ^{181}Ta, the presence of the defect Cd_{Ga}(Def) at room temperature prevents concise results with ^{111}Cd. As it would require detailed microscopic knowledge of the oxidation process around the probes and the resulting lattice parameters, the true thickness of the formed oxide layer is not directly accessible with this approach.

The validity of the above attribution of Cd_{Ga}(Ox) and Cd_{Ga}(Def) to probes on substitutional Ga_{II} lattice sites is checked in measurements at various sample temperatures ranging from 19 K to 973 K. These show that Cd_{Ga}(Def) represents a purely electronic defect which can be trapped or de-trapped depending on the temperature. They furthermore show that Cd_{Ga}(Ox) is especially pronounced both at temperatures below 150 K and above 750 K, but suppressed between room temperature and 600 K. We adapt a model of self-trapped holes in Ga_2O_3 for both the high and low temperature behavior of the Cd_{Ga}(Ox) and Cd_{Ga}(Def) interplay, which could be checked by additional temperature-dependent PAC measurements or ab-initio simulations on Cd-doped materials where self-trapped holes are expected.

References

1. Weng, W., Hsueh, T., Chang, S., Huang, G., Hsueh, H.: IEEE Sensors J. **11**(4), 999 (2011). doi:10.1109/JSEN.2010.2062176

2. Frauenfelder, H.: Annu. Rev. Nucl. Sci **2**(1), 129 (1953). doi:10.1146/annurev.ns.02.120153.001021
3. Blachot, J.: Nucl. Data Sheets **110**(6), 1239 (2009). doi:10.1016/j.nds.2009.04.002
4. Wu, S.: Nucl. Data Sheets **106**(3), 367 (2005). doi:10.1016/j.nds.2005.11.001
5. Valentini, R., Vianden, R.: Nuclear Instruments and Methods in Physics Research Section A: Accelerators, Spectrometers, Detectors and Associated Equipment **623**(4), 1002 (2010). doi:10.1016/j.nima.2010.07.084
6. Haaks, M., Valentini, R., Vianden, R.: Phys. Status Solidi C **4**, 4036 (2007). doi:10.1002/pssc.200675869
7. Biersack, J.P., Haggmark, L.G.: Nucl. Instrum. Meth. **174**(1–2), 257 (1980). doi:10.1016/0029-554X(80)90440-1
8. Ronning, C., Carlson, E., Davis, R.: Phys. Rep. **351**(5), 349 (2001). doi:10.1016/S0370-1573(00)00142-3
9. King, S.W., Barnak, J.P., Bremser, M.D., Tracy, K.M., Ronning, C., Davis, R.F., Nemanich, R.J.: J. Appl. Phys. **84**(9), 5248 (1998). doi:10.1063/1.368814. http://link.aip.org/link/?JAP/84/5248/1
10. Zhuang, D., Edgar, J.: Mater. Sci. Eng. R. Rep. **48**(1), 1 (2005). doi:10.1016/j.mser.2004.11.002. http://www.sciencedirect.com/science/article/pii/S0927796X04001251
11. Forker, M., Herz, W., Hütten, U., Müller, M., ßeler, R.M., Schmidberger, J., Simon, D., Weingarten, A., Bedi, S.C.: Nucl. Inst. Methods Phys. Res. A Accelerators, Spectrometers, Detectors and Associated Equipment **327**(2–3), 456 (1993). doi:10.1016/0168-9002(93)90711-P
12. Lorenz, K., Ruske, F., Vianden, R.: Phys. Status Solidi B **228**(1), 331 (2001). doi:10.1002/1521-3951(200111)228:1<331::AID-PSSB331>3.0.CO;2-6
13. Kessler, P., Lorenz, K., Vianden, R.: Def. Diff. Forum **311**, 167 (2011). doi:10.4028/www.scientific.net/DDF.311.167
14. Lorenz, K., Geruschke, T., Alves, E., Vianden, R.: Hyperfine Interact **177**, 89 (2007). doi:10.1007/s10751-008-9708-7
15. Bartels, J., Freitag, K., Marques, J., Soares, J., Vianden, R.: Hyperfine Interact **120-121**, 397 (1999). doi:10.1023/A:1017080902893
16. Shitu, J., Pasquevich, A.F.: J. Phys. Condens. Matter **9**(29), 6313 (1997). doi:10.1088/0953-8984/9/29/016
17. Blanco, M.A., Sahariah, M.B., Jiang, H., Costales, A., Pandey, R.: Phys. Rev. B **72**, 184103 (2005). doi:10.1103/PhysRevB.72.184103
18. Pasquevich, A.F., Uhrmacher, M., Ziegeler, L., Lieb, K.P.: Phys. Rev. B **48**, 10052 (1993). doi:10.1103/PhysRevB.48.10052
19. Pasquevich, A.: Hyperfine Interact **60**, 791 (1990). doi:10.1007/BF02399871
20. Alves, E., da Silva, M., Marques, J., Soares, J., Freitag, K.: Mater. Sci. Eng. B **59**(1–3), 207 (1999). doi:10.1016/S0921-5107(98)00392-4
21. López, I.N., Utrilla, A.D., Nogales, E., Méndez, B., Piqueras, J., Peche, A., Ramírez-Castellanos, J., González-Calbet, J.M.: J. Phys. Chem. C **116**(6), 3935 (2012). doi:10.1021/jp210233p
22. Jacobs, V.L., Rozsnyai, B.F.: Phys. Rev. A **34**, 216 (1986). doi:10.1103/PhysRevA.34.216
23. Haas, H., Shirley, D.A.: J. Chem. Phys. **58**(8), 3339 (1973). doi:10.1063/1.1679661
24. Sevik, C., Bulutay, C.: Phys. Rev. B **77**, 125414 (2008). doi:10.1103/PhysRevB.77.125414
25. Varley, J.B., Janotti, A., Franchini, C., Van de Walle, C.G.: Phys. Rev. B **85**, 081109 (2012). doi:10.1103/PhysRevB.85.081109
26. Åhman, J., Svensson, G., Albertsson, J.: Acta Crystallogr., Sect. C: Cryst. Struct. Commun. **52**(6), 1336 (1996). doi:10.1107/S0108270195016404
27. Harwig, T., Kellendonk, F., Slappendel, S.: J. Phys. Chem. Solids **39**(6), 675 (1978). doi:10.1016/0022-3697(78)90183-X
28. Armstrong, A.M., Crawford, M.H., Jayawardena, A., Ahyi, A., Dhar, S.: J. Appl. Phys. **119**(10), 103102 (2016). doi:10.1063/1.4943261
29. Onuma, T., Fujioka, S., Yamaguchi, T., Higashiwaki, M., Sasaki, K., Masui, T., Honda, T.: Appl. Phys. Lett. **103**(4), 041910 (2013). doi:10.1063/1.4816759
30. Pasquevich, A.F., Rentería, M.: Def. Diff. Forum **311**, 62 (2011). doi:10.4028/www.scientific.net/DDF.311.62